PERGAMON

Computers & Geosciences 29 (2003) 195–207

COMPUTERS & GEOSCIENCES

www.elsevier.com/locate/cageo

Computation of deformation induced by earthquakes in a multi-layered elastic crust—FORTRAN programs EDGRN/EDCMP ☆

Rongjiang Wang[a,*], Francisco Lorenzo Martín[b], Frank Roth[a]

[a] GeoForschungsZentrum Potsdam (GFZ), Telegrafenberg, D-14473 Potsdam, Germany
[b] Institute of Geology, Mineralogy and Geophysics, Ruhr University Bochum, D-44780 Bochum, Germany

Received 18 March 2002; received in revised form 4 September 2002; accepted 5 September 2002

Abstract

This is the first article in a series in which we introduce methods to determine the permanent and transient deformation induced by earthquakes or similar sources. The point-like and extended foci can be located in a stratified elastic half-space. The software includes a tool to combine the sources to one or more extended sources with arbitrary strike and dip. The number of layers is essentially not limited. The output covers surface and subsurface displacements, strain, tilt and stress. Several effective techniques have been used to solve the stability and convergence problems in computation of the Green's functions, so that the programs are small, fast and accurate. To control the accuracy of the numerical results, the software provides an optional link to Okada's analytical solutions in the special case of a homogeneous half-space. This can also be used for creating zeroth order approaches, i.e. starting models.

Keywords: Dislocation theory; Propagator algorithm; Hankel transform; Green's function; Numerical stability

1. Introduction

As the number of stations and campaigns using the global positioning system (GPS) increases and, at the same time, more Interferograms of Synthetic Aperture Radar (INSAR) data are generated, crustal deformation has become visible with higher accuracy and in shorter time intervals. This poses more stringent requirements to the software used to model the observed movements.

This paper, as one in a series, introduces methods that serve this purpose with a common theoretical, transparent basis and software that presents similar front-ends for the users. This article covers (1) earthquakes' static deformation, and following ones will cover (2) deterministic simulation of seismic ground motion (synthetic seismograms), (3) inelastic post-seismic creep, and (4) coupled diffusion and deformation in poro-elastic media.

In all situations, a horizontally layered medium is used, where the number of layers is effectively unlimited, the layer thickness is arbitrary, and the material parameters (in the present example they are the two Lamé constants) can be chosen independently from each other. This provides the possibility to incorporate detailed information available on the Earth's structure provided e.g. by deep seismic sounding. The sources cover all those frequently encountered in geophysics as double-couples, single forces, inflations, etc. The software supports superposition of these point sources to model realistic earthquake's fault planes with changes in strike, dip and slip and even the determination of the combined effect of several earthquakes separated in space and time. These refined models are part of the necessary response to the higher accuracy in deformation data.

☆ Code available from server at http://www.iamg.org/CGEditor/index.htm.

*Corresponding author.
E-mail address: wang@gfz-potsdam.de (R. Wang).

0098-3004/02/$ - see front matter
PII: S0098-3004(02)00111-5

For static elastic deformation in a layered half-space, there exists a number of published numerical techniques and software. Most of them are based on the wavenumber integration method. Table 1 provides an overview. From the beginning it was clear that—in contrast to the homogeneous half-space—the wavenumber spectra or kernel functions obtained for the stratified case could not be integrated analytically. Two directions were followed to solve this: (i) numerical integration (cf. Sato, 1971; Sato and Matsu'ura, 1973) and (ii) approximation by a finite series of Lipshitz–Hankel integrals in a recursive algorithm suggested by Sneddon (1951) and first applied here by Ben-Menahem and Gillon (1970) (see also Jovanovich et al., 1974a; Roth, 1983). At the same time, it also became clear that the number of calculations for the kernel functions increase exponentially with the number of layers if the analytical approach is used. This is due to the fact that—similar to the propagation of seismic waves—the deformation is reflected and converted (P- into S-type motions and vice versa) at every layer boundary leading to a large number of 'multiples' the farther the motion travels. Therefore, the previous algorithms based on the analytical or semi-analytical methods were essentially limited to no more than four layers over the half-space (cf. Roth, 1992). Another way for computing the kernel functions was to adopt the propagator algorithm which was first applied by Thomson (1950) and Haskell (1953) to seismic wave propagation in layered media. Though the formulation of the propagator algorithm was transparent and could be applied to any unlimited number of layers, its numerical results also showed the instability as known from dynamic solutions (see for instance Sato, 1971). To overcome these, mathematical improvements in the algorithm were introduced, cf. Dunkin (1965), Jovanovich et al. (1974a), and Roth (1983). Their success was clearly visible but nevertheless limited. This did not change until Wang (1999b) approached the problem from a physical point of view, as summarised in the next section.

2. The method

The Green's function approach is used to solve the present boundary-value problem. Using the Hankel transform, the partial differential equations of motion are converted into a set of ordinary equations governing the deformation field in the wavenumber domain. For each homogeneous layer, all fundamental solutions of the latter equation are given in closed analytical form. The special solution satisfying the source and boundary conditions will be obtained by the Thomson–Haskell propagator algorithm. When the wavenumber domain problem has been solved, the desired deformation field in the spatial domain is then obtained through the inverse Hankel transform. In general, Green's functions are calculated for three different types of point double-couple dislocations so that any finite dislocation can be modelled via linear superposition. Theoretically, all calculations in the propagator algorithm are based on analytical formulae. Only the inverse Hankel transform has to be carried out numerically. In practice, however, numerical problems appear in both procedures above. After the basic theory is outlined, this section will concentrate on the numerical techniques used in the present software.

2.1. Description of the boundary-value problem

The partial differential equations governing the static deformation in an elastic medium are given by the equilibrium conditions of linear momentum,

$$\nabla \cdot \mathbf{\Gamma} = \mathbf{f}, \tag{1}$$

where $\mathbf{\Gamma}$ is the stress tensor, and $\mathbf{f}$ is the body force. In combination with the Hooke's law

$$\mathbf{\Gamma} = (\lambda \nabla \cdot \mathbf{u})\mathbf{I} + \mu[\nabla \mathbf{u} + (\nabla \mathbf{u})^{\mathrm{T}}], \tag{2}$$

the governing equations can be written in terms of displacements of the medium,

$$(\lambda + 2\mu)\nabla(\nabla \cdot \mathbf{u}) - \mu \nabla \times (\nabla \times \mathbf{u}) = \mathbf{f}, \tag{3}$$

where λ and μ are the two Lamé constants, $\mathbf{u}$ is the displacement vector, and $\mathbf{I}$ is the unit tensor.

At an interior material interface, displacement and stress satisfy the continuity conditions:

$$\mathbf{u}|_{-}^{+} = \mathbf{0} \tag{4}$$

$$\mathbf{e}_n \cdot \mathbf{\Gamma}|_{-}^{+} = \mathbf{0}, \tag{5}$$

where $\mathbf{e}_n$ is the unit normal vector of the interface, and the symbol $|_{-}^{+}$ denotes the increment of the respective quantity from one side to the other side of the interface. The free surface is expressed by

$$\mathbf{e}_n \cdot \mathbf{\Gamma} = \mathbf{0}. \tag{6}$$

In the Green's function approach, the function $\mathbf{f}$ describes a point source. For convenience in numerical calculations, the plane at the source depth will be defined as a pseudo-interface. Then, the point source can be represented by a jump of the displacement and stress components. In case that $\mathbf{f} = \mathbf{f}_s \delta(z - z_s)$, for example, the source is then represented by a stress jump through the horizontal plane at $z = z_s$,

$$\mathbf{e}_n \cdot \mathbf{\Gamma}|_{-}^{+} = \mathbf{f}_s. \tag{7}$$

2.2. Application of the Hankel transform

For a layered half-space model which consists of an arbitrary but finite number of horizontal layers with a free surface on top and the deepest layer extending to

infinite depth, it is convenient to use the cylindrical coordinate system $\mathbf{x} = (z, r, \theta)$ in which z is the symmetry axis through the point source and positive downwards. Consider the Hankel transforms (e.g. Aki and Richards, 1980, p. 305):

$$\mathbf{u}(z,r,\theta) = \sum_m \int_0^\infty [U_m(z,k)\,\mathbf{Z}_k^m(r,\theta) + V_m(z,k)\,\mathbf{R}_k^m(r,\theta) + W_m(z,k)\,\mathbf{T}_k^m(r,\theta)]k\,\mathrm{d}k, \tag{8}$$

$$\mathbf{e}_z \cdot \boldsymbol{\Gamma}(z,r,\theta) = \sum_m \int_0^\infty [E_m(z,k)\,\mathbf{Z}_k^m(r,\theta) + F_m(z,k)\,\mathbf{R}_k^m(r,\theta) + G_m(z,k)\mathbf{T}_k^m(r,\theta)]k\,\mathrm{d}k, \tag{9}$$

where U_m, V_m, … are the wavenumber spectra of the stress and displacement field,

$$Y_k^m(r,\theta) = J_m(kr)\begin{pmatrix}\cos m\theta \\ \sin m\theta\end{pmatrix} \tag{10}$$

$(0 \leqslant k < \infty,\ m = 0, 1, 2, \ldots)$, are the cylindrical surface harmonics, and

$$\mathbf{Z}_k^m(r,\theta) = \mathbf{e}_z\, Y_k^m(r,\theta), \tag{11}$$

$$\mathbf{R}_k^m(r,\theta) = \left(\frac{\mathbf{e}_r}{k}\frac{\partial}{\partial r} + \frac{\mathbf{e}_\theta}{kr}\frac{\partial}{\partial\theta}\right) Y_k^m(r,\theta), \tag{12}$$

$$\mathbf{T}_k^m(r,\theta) = \left(\frac{\mathbf{e}_r}{kr}\frac{\partial}{\partial\theta} - \frac{\mathbf{e}_\theta}{k}\frac{\partial}{\partial r}\right) Y_k^m(r,\theta) \tag{13}$$

are the corresponding surface vector harmonics. For a point inflation, only the harmonics of degree $m = 0$ are needed; for a single force, $m = 0, 1$; for a double couple source, $m = 0, 1, 2$; and so on. Application of the Hankel transform to Eqs. (3) yields two systems of ordinary differential equations which are decoupled from each other and govern the depth-dependent coefficient sets (U_m, E_m, V_m, F_m) and (W_m, G_m), respectively.

The first system is called the poloidal mode and corresponds to the P–SV wave field in seismology. In the matrix notation it can be written as

$$\frac{\mathrm{d}}{\mathrm{d}z}\mathbf{y}_m = \mathbf{A}\mathbf{y}_m, \tag{14}$$

where

$$\mathbf{y}_m = (U_m, E_m, V_m, F_m)^{\mathrm{T}} \tag{15}$$

expresses a generalised 4D displacement vector in the wavenumber domain, and

$$\mathbf{A} = \begin{pmatrix} 0 & \frac{1}{\xi} & \frac{\lambda k}{\xi} & 0 \\ 0 & 0 & 0 & k \\ -k & 0 & 0 & \frac{1}{\mu} \\ 0 & -\frac{\lambda k}{\xi} & \frac{4k^2\mu\eta}{\xi} & 0 \end{pmatrix} \tag{16}$$

is the coefficient matrix with

$$\xi = \lambda + 2\mu, \tag{17}$$

$$\eta = \lambda + \mu. \tag{18}$$

The second system is a 2D toroidal mode corresponding to the SH wave field in seismology,

$$\frac{\mathrm{d}}{\mathrm{d}z}\mathbf{x}_m = \mathbf{B}\mathbf{x}_m, \tag{19}$$

where

$$\mathbf{x}_m = (W_m, G_m)^{\mathrm{T}} \tag{20}$$

and

$$\mathbf{B} = \begin{pmatrix} 0 & \frac{1}{\mu} \\ -\mu k^2 & 0 \end{pmatrix}. \tag{21}$$

The interface conditions (4) and (5) are then expressed by the continuity conditions of the generalised displacement vectors $\mathbf{y}_m$ and $\mathbf{x}_m$,

$$\mathbf{y}_m|_-^+ = \mathbf{0}, \tag{22}$$

$$\mathbf{x}_m|_-^+ = \mathbf{0}, \tag{23}$$

the free surface conditions Eq. (6) by

$$\mathbf{y}_m = (U_m, 0, V_m, 0)^{\mathrm{T}}, \tag{24}$$

$$\mathbf{x}_m = (W_m, 0)^{\mathrm{T}} \tag{25}$$

and the source conditions in general by

$$\mathbf{y}_m|_-^+ = \Delta\mathbf{y}_m(z_s), \tag{26}$$

$$\mathbf{x}_m|_-^+ = \Delta\mathbf{x}_m(z_s), \tag{27}$$

where $\Delta\mathbf{y}_m(z_s)$ and $\Delta\mathbf{x}_m(z_s)$ are the poloidal and toroidal source functions, respectively. For a single force and a point dislocation, they are given in Appendix A.

2.3. Thomson–Haskell propagator algorithm

Solutions of Eqs. (14) and (19) are known in the closed analytical form. The poloidal displacement, for example, is expressed by

$$\mathbf{y}(z) = \mathbf{L}(z)\mathbf{E}(z)\mathbf{c}, \tag{28}$$

where $\mathbf{c}$ is a constant vector,

$$\mathbf{c} = (A_+, A_-, B_+, B_-)^{\mathrm{T}}, \tag{29}$$

$\mathbf{E}(z)$ is the (4×4) diagonal matrix

$$\mathbf{E}(z) = dia(\mathrm{e}^{kz}, \mathrm{e}^{-kz}, \mathrm{e}^{kz}, \mathrm{e}^{-kz}) \tag{30}$$

and $\mathbf{L}(z)$ is the (4×4) layer matrix given in Appendix B. Note that the displacement in the form of Eq. (28) shows again an analogy to seismology. The terms with constants $A_\pm$ and $B_\pm$ correspond to amplitudes of the up- and down-going P and SV waves, respectively. Their depth dependence is characterised by the terms $\mathrm{e}^{\pm kz}$ and $(kz)\mathrm{e}^{\pm kz}$, respectively.

Table 1
Published solutions for 3D static deformation induced by earthquakes in a layered half-space[a]

Publication	Source type				Source orientation			Source size	Deformation type	Number of layers[b]	Gravity[c] included (G)	Remarks
	Strike-slip	Dip-slip	Extens.	Explosion	Vertical	Horizontal	Inclined	Point (P) extended (E)				Displacement (D) or strain (S)
Ben-Menahem and Singh (1968)	X	X		X	X	X		P	D	2		(1)
Sato (1971)	X	X			X	X	X	E	D	7		
Singh (1971)	X	X		X	X			P	D	—		(2)
Wason and Singh (1972)	X	X		X	X			P	D	—		(3)
Sato and Matsu'ura (1973)	X	X		X	X	X	X	E	D	5		(4)
Jovanovich et al. (1974a)	X	X		X	X	X	X	P	D	4		
Jovanovich et al. (1974b)	X	X		X	X	X	X	P	S	5		(5)
Matsu'ura and Sato (1975)	X	X			X	X	X	E	S	5		(4)
Rundle (1980b)	X	X			X			P	D	—	G	(6)
Rundle (1981)	X	X			X			E	D	2	G	(6)
Rundle (1982)	X	X		X	X	X	X	E	D	2	G	(7)[d]
Roth (1983)	X	X		X	X	X	X	P	D & S	4		(8)[d]
Ma and Kusznir (1992)	X	X			X	X	X	E	D	4		(9)
Roth (1993)			X		X			P	D	3		(8)
Fernández and Rundle (1994b)				X	—	—	—	P	D	3	G	(10)
Ma and Kusznir (1994a)	X				X			E	D & S	4		[d]

Ma and Kusznir (1995)		X			X	X	X	E	D & S	4	G	[d]
Fernández et al. (1996b)		X			X	X	X	E	D	2	G	(11)[d]
Yu et al. (1996b)	X				X	X	X	E	D	2	G	(12)[d]
Fernández et al. (1997)				X	—	—	—	P	D & S	5	G	(13)
Wang (1999b)	X	X	X	X	X	X	X	P	D	~500		(14)
Fernández et al. (2001)				X	—	—	—	P	D	3	G	(15)[d]
This paper	X	X	X	X	X	X	X	E	D & S	~500		(16)

[a] If not stated otherwise, sources are discontinuities (dislocations) in displacement, Lamé's constants can be chosen independently, medium is elastic, and fields are given at surface.

[b] Layer number limit given in paper or maximum number of layers shown in an example. Half-space below layers is included in layer count. '—' Indicates that only formulae are given, but no examples.

[c] Gravity effects are included in one of two usually used approximations. For more details see Rundle (1980b) or Piersanti et al. (1997) for some overview.

[d] The modelling of inelastic behaviour is included, usually in some approximation. As this is beyond the scope of this paper see Roth (1994, table 4) for a more complete overview.

Notes: (1) Only the integrals are given for the displacements. (2) Here, sources are discontinuities in stress. Paper also treats dynamic case. (3) Medium is a layered sphere. Overview on this approach is not in scope of this paper, see Israel et al. (1973), Israel and Ben-Menahem (1974), Pollitz (1992), Sun and Okubo (1993), Okubo (1993, 1994), Piersanti et al. (1995), Pollitz (1996), Sun et al. (1996), Piersanti et al. (1997), Pollitz (1997), Sun and Okubo (1998), Wang (1999a), and Boschi et al. (2000) instead. (4) Rupture plane can extend through several layers, but see Morelli et al. (1987) or Bonafede and Rivalta (1999) for a more physical treatment. (5) Formulae for all surface strains and tilts are given (in cylindrical coordinates). (6) Displacements are given only integral form, solution of which can be found in Rundle (1980a). (7) Only vertical displacements are given integral form, the solution can be found in Rundle (1980a). (8) Later subsurface deformations were added (see Roth, 1990). Examples for 4 layers see also in Roth (1992, 1994). (9) Includes subsurface displacement and strain fields, elliptical source shapes, and variable slip distributions across the rupture plane; extended to visco-elastic gravitational media in Ma and Kusznir (1994b). (10) Program code published in Fernández and Rundle (1994a). (11) Only horizontal displacements. Program code published in Fernández et al. (1996a). (12) Program code published in Yu et al. (1996a). (13) Possibility to include a water layer at free surface. Besides strain also tilt can be computed. Includes program code. (14) Accuracy and performance was considerably increased with this algorithm (see text). Number of layers is practically not limited. Dynamic case is also treated. (15) More than one inelastic layer. (16) See footnote 14 for accuracy, performance and layer number.

For a homogeneous layer of thickness h, it is easy to find that the displacement at the lower boundary $z = h$ is related to its value at the upper boundary by

$$\mathbf{y}(h) = \mathbf{H}(h)\mathbf{y}(0), \tag{31}$$

where

$$\mathbf{H}(h) = \mathbf{L}(h)\mathbf{E}(h)\mathbf{L}^{-1}(0) \tag{32}$$

and $\mathbf{L}^{-1}(z)$ is the inverse of the layer matrix $\mathbf{L}(z)$. The matrix $\mathbf{H}$ is known as the Thomson–Haskell propagator that relates the displacement vector from depth to depth, so that the boundary-value problem is converted to an algebraic problem. In fact, we can choose any two independent starting values for the displacement vector, both of which satisfy the surface conditions ($E_m = F_m = 0$), and propagate it downwards until the source plane. The same procedure can be done from the deepest interface upwards to the source plane, the only difference is that the start values here should satisfy the conditions for infinity, that is, $A_+ = B_+ = 0$. The displacement vectors determined this way are the fundamental bases of solutions of the present boundary-value problem. The desired displacement is a linear superposition of them. The weights will be determined by the source conditions.

The situation for the toroidal mode is similar but easier than the poloidal mode shown previously because the dimension is reduced from 4 to 2. The (2×2) toroidal layer matrix is given in Appendix B.

2.4. The improved propagator algorithm

In practice, it has been shown that results for the toroidal mode are stable, but instable for the poloidal mode especially when the product between the wavenumber and the layer thickness is large. At first sight, the problem seems to be caused by operations between the large e^{kz} terms and the small e^{-kz} terms, but the stable results for the toroidal mode exclude this possibility. In reality, the problem is caused by operations between the two increasing vectors. For example, when a displacement vector is being propagated from the surface downwards (in the positive z direction), the terms A_+e^{kz} and $B_+(kz)e^{kz}$ represent two increasing waves and the terms A_-e^{-kz} and $B_-(kz)e^{-kz}$ two decreasing waves. It is obvious that through operations with the Thomson–Haskell propagator the two increasing waves included in the displacement vector become more significant than the two decreasing waves, in the extreme, i.e., when $kh \gg 1$, the latter can even lose their numerical presence. Additionally, also the less strongly increasing A_+e^{kz} wave, should have lost its significance to a certain extent due to the operation with the more strongly increasing $B_+(kz)e^{kz}$ wave. If such process is repeated by a number of thick layers, all displacement vectors may finally be dominated by the single $B_+(kz)e^{kz}$ wave, regardless what start values of them were chosen. Consequently, the fundamental displacement vector bases computed this way will loss their independence and the numerical instability arises when they are superposed to satisfy the source conditions.

From the physical point of view, the two decreasing e^{-kz} and $(kz)e^{-kz}$ waves describe the reflection from the top of a layer. When the layer thickness, measured by the wavelength $1/k$, is large enough, the evanescent reflection effect cannot be observed at the bottom of the layer. Thus, the vanishing of the decreasing waves is of physical nature. In contrast, however, the vanishing of one increasing wave due to operations with the other increasing wave is purely of numerical nature because both include independent and complementary information about the radiation characteristic of the source. Therefore, to solve the loss-of-precision problem, any direct numerical operations between the two increasing waves should be avoided. For this purpose, Wang (1999b) has proposed an orthonormalisation extension to the propagator algorithm. As has been stated, there are two fundamental displacement vector bases to be determined for the poloidal mode. In the improved propagator algorithm, the two vector bases are not computed separately but simultaneously. At each interface, they are linearly transformed, or orthonormalised in a wide sense, to the other two vector bases so that each of them includes only one increasing wave for the next homogeneous layer. Then, the new vector bases can be propagated to the next interface without any numerical operations between the two increasing waves and the loss-of-precision problem is fully solved.

The orthonormalised propagator algorithm has been successfully applied to the computation of synthetic seismograms (Wang, 1999b) and quasi-static deformations in poro-plastic media (Wang and Kümpel, 2002). The same computation strategy as demonstrated in the two papers is also adopted for the present purpose.

2.5. Convergence problems of the numerical Hankel transform

In the present software, the equidistant wavenumber sampling is used in the numerical Hankel transform (wavenumber integrations in Eqs. (8) and (9)). The sampling interval Δk can be chosen between 1% and 10% of the Nyquist wavenumber $2\pi/r_{max}$, where r_{max} is the maximum horizontal distance to the source. A practical problem here is the cut-off value of the wavenumber k, which depends upon how fast the integrands in Eqs. (8) and (9) converge to zero. In case that the observation points are located at a different depth than the source, the integrands decrease with wavenumber k approximately by e^{-kd} or ke^{-kd}, where d is the depth difference between the observation points and the source. Then, the cut-off wavenumber can be

determined so that all integrands become insignificant, for example, several orders smaller than their maxima. However, if the source and the observation points are located at the same depth, the integrands at large wavenumbers either converge to non-zero constants or linearly increase with the wavenumber. The difficulty is caused by the idealized point source and can be solved using a similar technique as the one used by Farrell (1972) for calculating the deformation of a spherical earth induced by surface loading. Using this technique, the asymptotic terms are expressed in the analytical form and removed from the numerical wavenumber integrations. In addition, the δ point source function is replaced by an extended disk source with a characteristic radius r_o which is much smaller than the distance to the observation points. For example, if an extended source with a normal distribution is used, the only difference to the point source is an additional factor $e^{-k^2 r_o^2}$ to be multiplied to the wavenumber integrands. In practice, this factor can effectively accelerate the convergence of the numerical integrations. The following example demonstrates how the convergence problem is solved:

$$\begin{aligned}
&\int_0^\infty U(k)J_2(kr)k\,\mathrm{d}k \\
&\quad = \int_0^\infty \Delta U(k)J_2(kr)k\,\mathrm{d}k + U_\infty \int_0^\infty J_2(kr)k\,\mathrm{d}k \\
&\quad = \int_0^\infty \Delta U(k)J_2(kr)k\,\mathrm{d}k + \frac{2}{r^2}U_\infty \\
&\quad \approx \int_0^{k_\infty} \Delta U(k)J_2(kr)e^{-k^2 r_o^2}k\,\mathrm{d}k + \frac{2}{r^2}U_\infty, \qquad (33)
\end{aligned}$$

where U_∞ is the limit value of $U(k)$ for $k \to \infty$, $\Delta U(k)$ is the difference $U(k) - U_\infty$, k_∞ is the cut-off wavenumber, and $r_o \ll r$ is the characteristic spatial extension of the physical point source. Presently, k_∞ is determined through a rough sampling so that the integrands decrease by 3–4 orders for $k > k_\infty$ in comparison with their maxima, and r_o is about 1% of the source–observation distance r.

3. The computation procedures

The present software comprises two programs: EDGRN prepares the Green's functions and EDCMP computes the desired deformation field via linear superposition. The flowcharts of major subroutines of the two programs are shown in Figs. 1 and 2, respectively.

For a general dislocation source, Green's functions for three independent source types are needed, that is, the compensated linear vector dipole (abbreviated by CLVD), the dip-slip, and the strike-slip double couples. There are 10 observables to be computed with the program EDGRN: 3 displacement components, 6 strain components and the radial component of the surface tilt (its tangential component is given by the azimuthal derivative of the vertical displacement). For a fixed uniform observation depth, the observables depend, in general, not only on the source depth and the observation distance but also on the observation azimuth angle θ. Fortunately, the azimuth dependence is quite regular. Except for the axi-symmetric CLVD source, the azimuthal dependence for the other two source types can be expressed by a simple azimuthal factor, that is, $(\sin 2\theta, \cos 2\theta)$ for the strike-slip source and $(\sin\theta, \cos\theta)$ for the dip-slip source. Whether the cosine factor or the sine factor is used depends on which of the observables is considered. In case of the dip-slip source ($M_{xz} \neq 0$), for

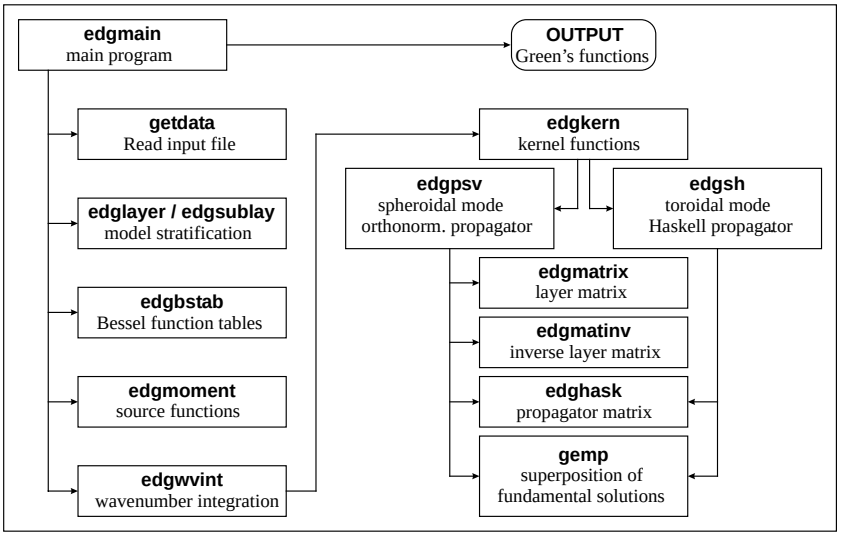

Fig. 1. Flowchart of major subroutines of program EDGRN.

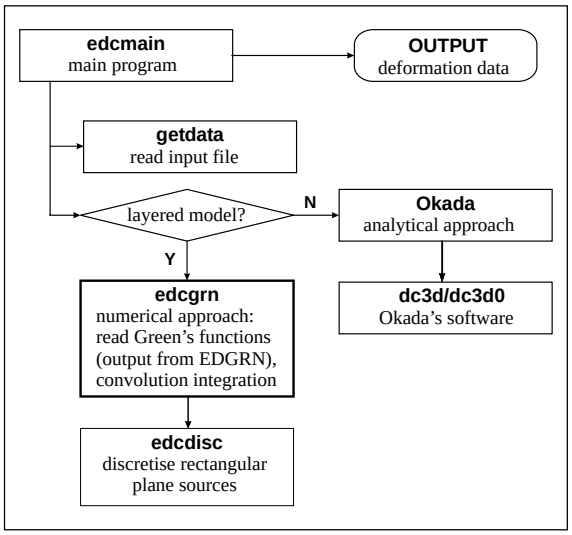

Fig. 2. Flowchart of major subroutines of program EDCMP.

example, both the vertical and radial displacements are proportional to $\cos\theta$, but the tangential displacement is proportional to $\sin\theta$. The Green's functions are thus stored without the azimuthal factor. The stepping of source depths and observation distances should be dense enough so that a linear interpolation can be applied later to any individual source–observation configurations. In practice, the step should be comparable with the discretisation size to be applied later to the finite source plane. Output data files include several header lines with information about the source type, the source depths, the observation distances, the observables and their unit, etc.

In the next step, the user can approximate the earthquake source by a few rectangular dislocation planes. Each is defined by 9 parameters: the slip, the Cartesian coordinates (x, y, z) of the reference point, the length, the width, and the strike, dip and rake angles. The program EDCMP automatically discretises the rectangles to a number of point sources, and then calculates up to 17 different physical observables for the given observation positions via linear superposition. In addition, the program EDCMP provides an optional link to the subroutines of Okada (1992) giving the analytical results in case of the homogeneous half-space model.

The program codes are written in the FORTRAN77 language with some extensions which are accepted by most present FORTRAN compilers. A short READ.ME file gives all necessary information for the installation and a brief introduction to the theoretical background. Both programs EDGRN and EDCMP read the input parameters from input files. The examples edgrn.inp and edcmp.inp for the two input files, respectively, are supplied with the codes. They include sufficient explanations for all input parameters. Users can modify the parameter values for their own applications.

4. An application example

The example as given in the provided two input files demonstrates the computation of the elastic deformation field induced by the 1999 Izmit earthquake, Turkey. The fault plane of the earthquake consists of 6 rectangular segments which are adopted from Wright et al. (2001). The nearly E–W-trending fault has a total length of about 140 km. Its depth extends from the surface to 20 km. The Green's functions are computed by the program EDGRN for 43 source depths (every 0.5 km from 0 to 21 km) and for 401 distances (every 0.5 km from 0 to 200 km), that is, $43 \times 401 = 17,243$ source–observation combinations. The CPU time on a SUN Ultra-60 Workstation is 72–77 s, depending on whether a homogeneous or a 4-layers model is used.

Once the Green's functions have been prepared, the stress and displacement components can be computed by the program EDCMP either for a 2D observation array, for a 1D observation profile, or for a number of irregular observation positions. In case of a layered earth model, the program first discretises the 6 finite dislocation rectangles to 10,880 point sources for a grid size 0.5 km $\times$ 0.5 km, and then computes the deformation field via linear superposition. The CPU time for this part of the computations on the same SUN workstation is 447 s for a 2D array with 6161 stations (Fig. 3) or 16 s for a 1D profile with 201 stations (Fig. 4). That is about 80 ms each station. If a homogeneous half-space model is considered, however, the problem can be optionally solved using the Okada's analytical approach. In this case, the Green's functions as well as the discretisation of the finite dislocation rectangles are not needed and the results can be obtained immediately.

Fig. 3 shows the computed surface displacements for a homogeneous half-space and a 4-layers half-space. The elasticity parameters of the 4-layers model are given in Table 2 (note that the input parameters for the model are the density ρ and the two seismic velocities V_p and V_s instead of the two Lamé constants λ and μ). The homogeneous model takes the same elasticity parameters as the uppermost layer of the stratified model. This kind of modelling is useful for interpreting the GPS and INSAR data. To control the numerical accuracy, the results for the homogeneous half-space are compared with the Okada's analytical solutions (Fig. 4). A few visible deviations are only found near the surface fault traces and are mainly caused by the finite grid size used for the source plane discretisation.

The example shown above is a hard test for the software. In fact, the extremely dense spatial sampling is only necessary when the near-field deformation of

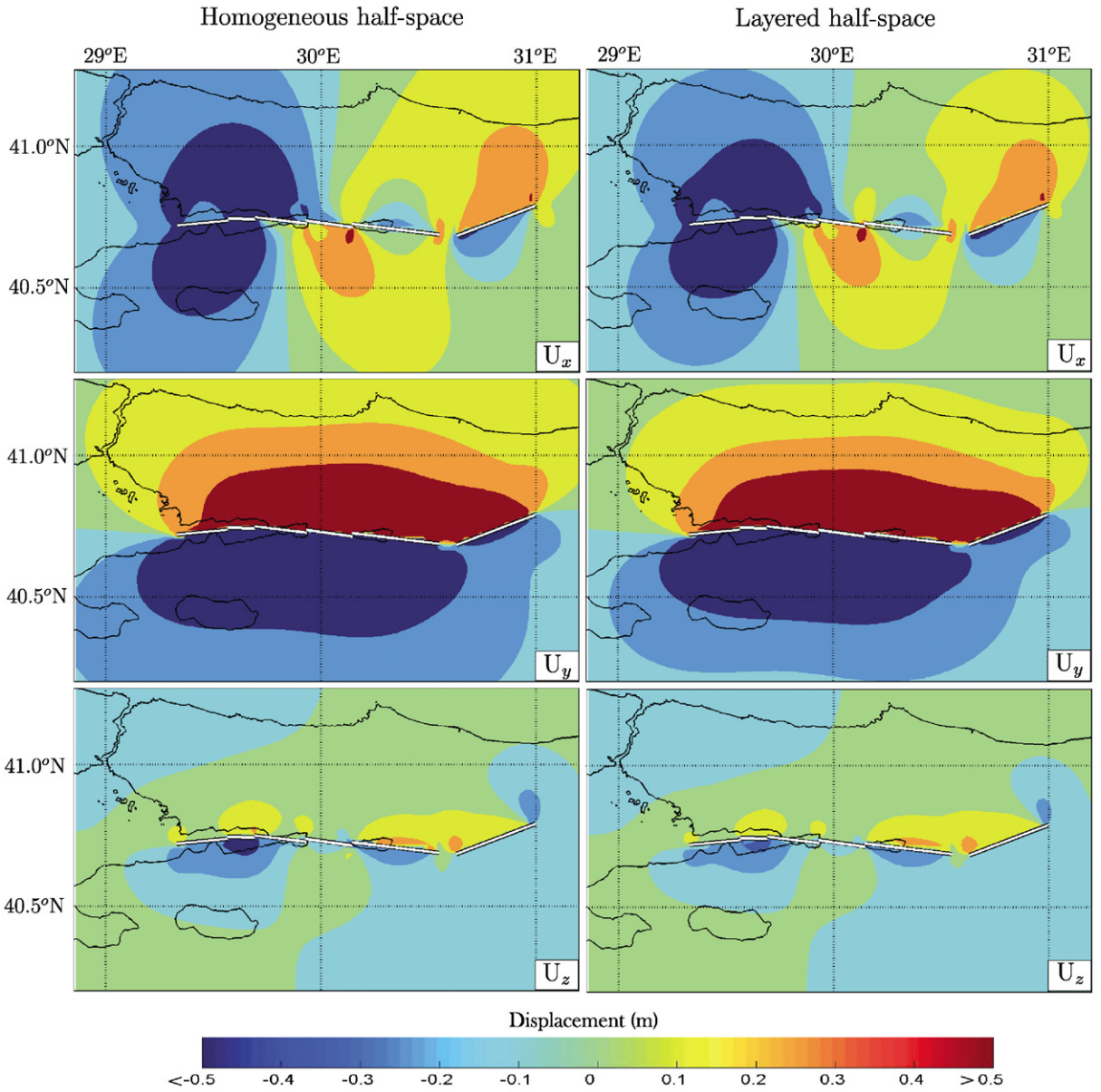

Fig. 3. Surface displacements (m) induced by August 17, 1999, Izmit earthquake, Turkey, computed with present software using numerical Green's function method. Earthquake has an E–W-trending fault and consists of 6 segments whose parameters are adopted from Wright et al. (2001). Four-layer half-space model is given in Table 2. Homogeneous half-space model takes same elasticity parameters as uppermost layer of stratified model. Note that seismological convention for displacement components is used, that is, x is positive northwards, y is positive eastwards, and z is positive downwards.

shallow sources like the Izmit earthquake is considered. For far-field deformation or deeper earthquakes, the computation effort will be considerably smaller.

To check the ability of the method to handle models with a large number of layers, we added 100 pseudo-interfaces into the same homogeneous half-space model used above. The Green's functions computed by the program EDGRN did not change significantly ($<0.1\%$), but the CPU time on the same SUN Workstation increased from 72 to 158 s.

5. Conclusions

In the present software, the numerical Green's function approach is used to calculate earthquake's

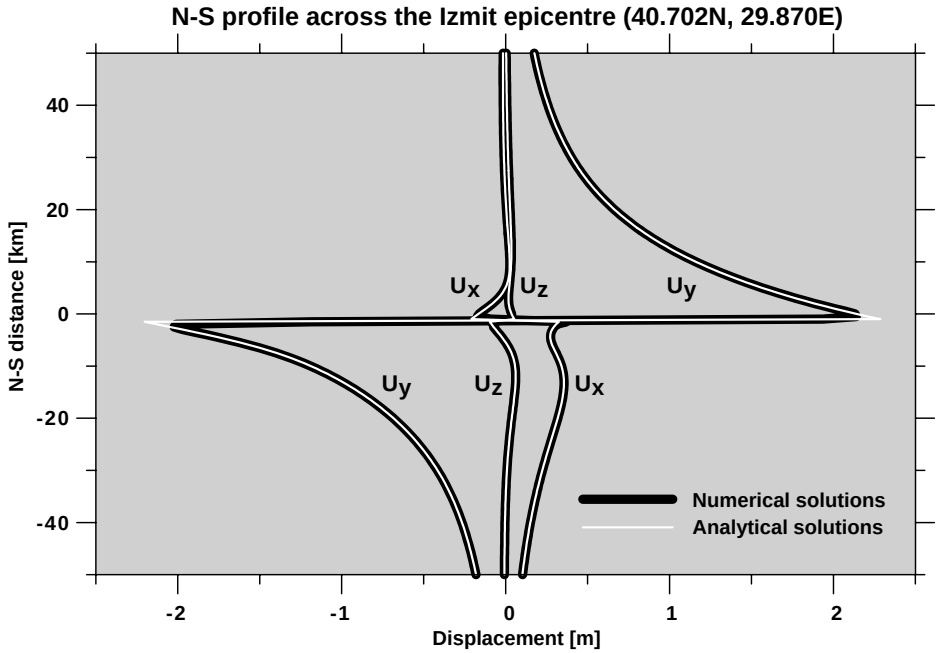

Fig. 4. Comparison of numerical results for homogeneous half-space with Okada's analytical solutions along a N–S profile across Izmit epicentre.

Table 2
Four-layers half-space model used in application example

Depth (km)	ρ (10^3 kg/m^3)	V_p (km/s)	V_s (km/s)	λ (10^{10} Pa)	μ (10^{10} Pa)
0–1	2.7	4.5	2.4	2.36	1.56
1–13	2.7	5.6	3.3	2.59	2.94
13–30	2.9	6.2	3.7	3.21	3.97
30–∞	3.3	7.9	4.6	6.64	6.98

elastic deformations based on a layered half-space earth model. In general, the computation task is fulfilled by two separate programs. The first program EDGRN prepares all fundamental Green's functions of the given multi-layered half-space, and the second program EDCMP carries out the convolution integrations. The advantage of this construction is the following: Once the Green's functions have been computed, they can be used repeatedly for different earthquakes as long as the earth model remains unchanged. In addition, when a homogeneous half-space model is used and the optional link provided by EDCMP to Okada's analytical subroutines is selected, the procedure for the Green's functions is not needed. In the program EDGRN, the stable and accurate results are guaranteed by the orthonormalised propagator algorithm, and the computation efficiency is achieved using the convergence accelerator technique applied to the numerical Hankel transform. Test examples have shown that the software can provide a quick and quasi-analytical solution of the elastic deformation induced by earthquake's dislocations in a multi-layered earth crust.

Acknowledgements

The authors are grateful to Prof. Okada for the kind permission to use his codes that provide the reference results in a special case. The work was supported by the GeoForschungsZentrum Potsdam, Ruhr-Univ. Bochum and the Deutsche Forschungsgemeinschaft under grant SFB 526 (Collaborative Research Centre 'Rheology of the Earth—from the Upper Crust to the Subduction Zone', subproject B2).

Table 3

Y_k^m	$J_m(kr)\cos m\theta$			$J_m(kr)\sin m\theta$	
m	0	1	2	1	2
ΔU_s	$-\frac{M_{zz}}{2\pi(\lambda+2\mu)}$	0	0	0	0
ΔV_m	0	$-\frac{M_{xz}}{2\pi\mu}$	0	$-\frac{M_{yz}}{2\pi\mu}$	0
ΔE_m	$\frac{f_z}{2\pi}$	0	0	0	0
ΔF_m	$\frac{(3\lambda+2\mu)M_{zz}}{2\pi(\lambda+2\mu)}k$	$\frac{f_x}{2\pi}$	$\frac{M_{xx}-M_{yy}}{4\pi}k$	$\frac{f_y}{2\pi}$	$\frac{M_{xy}}{2\pi}k$
ΔW_m	0	$\frac{M_{yz}}{2\pi\mu}$	0	$-\frac{M_{xz}}{2\pi\mu}$	0
ΔG_m	0	$-\frac{f_y}{2\pi}$	$-\frac{M_{xy}}{2\pi}k$	$\frac{f_x}{2\pi}$	$\frac{M_{xx}-M_{yy}}{4\pi}k$

Appendix A. Hankel transformed source functions

Table 3 shows the Hankel transformed source functions in the cases of a point single force (f_x, f_y, f_z) and a point dislocation with the moment tensor components $(M_{xx}, M_{xy}=M_{yx}, M_{xz}=M_{zx}, M_{yy}, M_{yz}=M_{zy}, M_{zz})$ with $M_{xx}+M_{yy}+M_{zz}=0$.

Appendix B. Layer matrices

The (4×4) poloidal layer matrix, whose 4 columns consist of the 4 eigenvectors of the coefficient matrix A given in Eq. (16), is

$$L(z) = \begin{pmatrix} 1 & 1 & 1+\frac{\lambda+\mu}{\mu}(1-kz) & 1+\frac{\lambda+\mu}{\mu}(1+kz) \\ 2\mu k & -2\mu k & 2(\lambda+\mu)(1-kz)k & -2(\lambda+\mu)(1+kz)k \\ 1 & -1 & -1-\frac{\lambda+\mu}{\mu}kz & 1-\frac{\lambda+\mu}{\mu}kz \\ 2\mu k & 2\mu k & -2(\lambda+\mu)k^2z & 2(\lambda+\mu)k^2z \end{pmatrix}. \tag{B.1}$$

The (2×2) toroidal layer matrix, whose 2 columns consist of the 2 eigenvectors of the coefficient matrix B given in Eq. (21), is

$$L(z) = \begin{pmatrix} 1 & 1 \\ \mu k & -\mu k \end{pmatrix}. \tag{B.2}$$

References

Aki, K., Richards, P.G., 1980. Quantitative Seismology, Vol. 1. W.H. Freeman, San Francisco, 558pp.

Ben-Menahem, A., Gillon, A., 1970. Crustal deformations by earthquakes and explosions. Bulletin of the Seismological Society of America 60, 193–215 (for remark on misprints see: Jovanovich, Husseini and Chinnery, Geophysical Journal of the Royal Astronomical Society 39, 210, 1974).

Ben-Menahem, A., Singh, S.J., 1968. Multipolar elastic fields in a layered half-space. Bulletin of the Seismological Society of America 58, 1519–1572 (for remark on misprints see: Jovanovich, Husseini and Chinnery, Geophysical Journal of the Royal Astronomical Society 39, 210, 1974).

Bonafede, M., Rivalta, E., 1999. The tensile dislocation problem in a layered elastic medium. Geophysical Journal International 136 (2), 341–356.

Boschi, L., Piersanti, A., Spada, G., 2000. Global postseismic deformation: deep earthquakes. Journal of Geophysical Research 105 (B1), 631–652.

Dunkin, J.W., 1965. Computation of modal solutions in layered elastic media at high frequencies. Bulletin of the Seismological Society of America 55, 335–358.

Farrell, W.E., 1972. Deformation of the earth by surface loads. Review of Geophysics and Space Physics 10 (3), 761–797.

Fernández, J., Rundle, J.B., 1994a. Fortran program to compute displacement, potential, and gravity changes resulting from a magma intrusion in a multilayered Earth model. Computers & Geosciences 20 (4), 461–510.

Fernández, J., Rundle, J.B., 1994b. Gravity changes and deformation due to a magmatic intrusion in a two-layered crustal model. Journal of Geophysical Research 99 (B2), 2737–2746.

Fernández, J., Rundle, J.B., Granell, R.D.R., Yu, T.-T., 1997. Programs to compute deformation due to a magma intrusion in elastic-gravitational layered earth models. Computers & Geosciences 23 (3), 231–249.

Fernández, J., Yu, T.-T., Rundle, J.B., 1996a. Deformation produced by a rectangular dipping fault in a viscoelastic-gravitational layered Earth model—Part I: thrust fault FLTGRV and FLTGRH FORTRAN programs. Computers & Geosciences 22 (7), 735–750 (corrections in: Computers & Geosciences 25 (3), 301–307, 1999).

Fernández, J., Yu, T.-T., Rundle, J.B., 1996b. Horizontal viscoelastic-gravitational displacement due to a rectangular dipping thrust fault in a layered Earth model. Journal of Geophysical Research 101, 13,581–13,594 (correction in Journal of Geophysical Research 103 (B12), 30283–30286, 1998).

Fernández, J., Tiampo, K.F., Rundle, J.B., 2001. Viscoelastic displacement and gravity changes due to point magmatic intrusions in a gravitational layered solid earth. Geophysical Journal International 146 (1), 155–170.

Haskell, N.A., 1953. The dispersion of surface waves on multilayered media. Bulletin of the Seismological Society of America 43, 17–34.

Israel, M., Ben-Menahem, A., 1974. Displacements and strains in real earth models. Physics of the Earth and Planetary Interiors 8, 23–45.

Israel, M., Ben-Menahem, A., Singh, S.J., 1973. Residual deformation of real Earth models with application to the Chandler wobble. Geophysical Journal of the Royal Astronomical Society 32, 219–247.

Jovanovich, D.B., Husseini, M.I., Chinnery, M.A., 1974a. Elastic dislocations in a layered half-space—I. Basic theory and numerical methods. Geophysical Journal of the Royal Astronomical Society 39, 205–217 (for remark on misprints see: Roth, Geophysical Journal International 103 (1), 155, 1990).

Jovanovich, D.B., Husseini, M.I., Chinnery, M.A., 1974b. Elastic dislocations in a layered half-space—II. The point source. Geophysical Journal of the Royal Astronomical Society 39, 219–239.

Ma, X.-Q., Kusznir, N.J., 1992. 3-D subsurface displacement and strain fields for faults and fault arrays in a layered elastic half-space. Geophysical Journal International 111, 542–558.

Ma, X.-Q., Kusznir, N.J., 1994a. Coseismic and postseismic subsurface displacements and strains for a vertical strike-slip fault in a three-layer elastic medium. Pure and Applied Physics 142, 687–709.

Ma, X.-Q., Kusznir, N.J., 1994b. Effects of rigidity layering, gravity and stress relaxation on 3-D subsurface fault displacement fields. Geophysical Journal International 118, 201–220.

Ma, X.-Q., Kusznir, N.J., 1995. Coseismic and postseismic subsurface displacements and strains for a dip-slip normal fault in a three-layer elastic-gravitational medium. Journal of Geophysical Research 100, 12813–12830.

Matsu'ura, M., Sato, R., 1975. Static deformations due to the fault spreading over several layers in a multilayered medium. Part II. Strain and tilt. Journal of Physics of the Earth 23, 1–29.

Morelli, A., Bonafede, M., Dragoni, M., 1987. Two-dimensional crack model of faulting in a layered elastic half-space. Annales Geophysicae 5B, 281–288.

Okada, Y., 1992. Internal deformation due to shear and tensile faults in a half-space. Bulletin of the Seismological Society of America 82, 1018–1040.

Okubo, S., 1993. Reciprocity theorem to compute the static deformation due to a point dislocation buried in a spherically symmetric earth. Geophysical Journal International 115, 921–928.

Okubo, S., 1994. Coseismic crustal movement in a spherically symmetric earth. Proceedings of the Eighth International Symposium on Recent Crustal Movements (CRCM '93) of IUGG and IAG, December 6–11, 1993, The Local Organizing Committee for the CRCM '93, Kobe, pp. 275–278.

Piersanti, A., Spada, G., Sabadini, R., 1997. Global postseismic rebound of a viscoelastic Earth: theory for finite faults and application to the 1964 Alaska earthquake. Journal of Geophysical Research 102, 477–492.

Piersanti, A., Spada, G., Sabadini, R., Bonafede, M., 1995. Global post-seismic deformation. Geophysical Journal International 120, 544–566.

Pollitz, F.F., 1992. Postseismic relaxation theory on the spherical earth. Bulletin of the Seismological Society of America 82, 422–453.

Pollitz, F.F., 1996. Coseismic deformation from earthquake faulting on a layered spherical earth. Geophysical Journal International 125, 1–14.

Pollitz, F.F., 1997. Gravitational viscoelastic postseismic relaxation on a layered spherical Earth. Journal of Geophysical Research 102 (B8), 17,921–17,941.

Roth, F., 1983. Oberflächendeformationen und Krustenspannungen in Erdbebengebieten: Ein Modell zur Beschreibung ihrer zeitlichen Änderungen. Dissertation, Institut. fuer. Geophys., C.-A.-Univ. Kiel, Germany, 184p.

Roth, F., 1990. Subsurface deformations in a layered elastic half-space. Geophysical Journal International 103 (2), 147–155.

Roth, F., 1992. Modellierung von Vorgängen an Verwerfungen mit Hilfe der Dislokationstheorie. Habilitationsschrift, Berichte Reihe A, 35, Institut fuer Geophysik, Ruhr-Univ. Bochum, Germany, 196p.

Roth, F., 1993. Deformations in a layered crust due to a system of cracks: modelling the effect of dike injections or dilatancy. Journal of Geophysical Research 98, 4543–4551.

Roth, F., 1994. New methods using dislocation theory. Proceedings of the Eighth International Symposium on Recent Crustal Movements (CRCM '93) of IUGG and IAG, The Local Organizing Committee for the CRCM '93, Kobe, December 6–11, 1993, Journal of the Geodetic Society of Japan (special issue), pp. 265–274.

Rundle, J.B., 1980a. Numerical evaluation of a static elastic-gravitational deformation of a layered half-space by point couple-sources. Report, Sandia National Laboratory, Albuquerque, NM, SAND 80-2048.

Rundle, J.B., 1980b. Static elastic-gravitational deformation of a layered half space by point couple sources. Journal of Geophysical Research 85, 5355–5363.

Rundle, J.B., 1981. Vertical displacements from a rectangular fault in layered elastic-gravitational media. Journal of Physics of the Earth 29, 173–186.

Rundle, J.B., 1982. Viscoelastic-gravitational deformation by a rectangular thrust fault in a layered Earth. Journal of Geophysical Research 87, 7787–7796.

Sato, R., 1971. Crustal deformation due to a dislocation in a multi-layered medium. Journal of Physics of the Earth 19, 31–46.

Sato, R., Matsu'ura, M., 1973. Static deformation due to the fault spreading over several layers in a multi-layered medium. Part I: displacement. Journal of Physics of the Earth 21, 227–249.

Singh, S.J., 1971. Deformation of a multilayered half-space by stress dislocations and concentrated forces. Bulletin of the Seismological Society of America 61, 1625–1637.

Sneddon, I.N., 1951. Fourier Transforms. McGraw-Hill, New York, 542pp.

Sun, W., Okubo, S., 1993. Surface potential and gravity changes due to internal dislocations in a spherical earth—I. Theory for a point dislocation. Geophysical Journal International 114, 569–592.

Sun, W., Okubo, S., 1998. Surface potential and gravity changes due to internal dislocations in a spherical earth—II. Application to a finite fault. Geophysical Journal International 132 (1), 79–88.

Sun, W., Okubo, S., Vaníček, P., 1996. Global displacements caused by point dislocations in a realistic Earth model. Journal of Geophysical Research 101, 8561–8578.

Thomson, W.T., 1950. Transmission of elastic waves through a stratified medium. Journal of Applied Physics 21, 89–93.

Wang, H., 1999a. Surface vertical displacements, potential perturbations and gravity changes of a viscoelastic earth model induced by internal point dislocations. Geophysical Journal International 137 (2), 429–440.

Wang, R., 1999b. A simple orthonormalization method for the stable and efficient computation of Green's functions. Bulletin of the Seismological Society of America 89, 733–741.

Wang, R., Kümpel, H.-J., 2002. Poroelasticity: axisymmetric solutions for the uniform and the layered half-space. Geophysics, in press.

Wason, H.R., Singh, S.J., 1972. Static deformation of multi-layered sphere by internal sources. Geophysical Journal of the Royal Astronomical Society 27, 1–14.

Wright, T., Fielding, E., Parsons, B., 2001. Triggered slip: observations of the 17 August 1999 Izmit (Turkey) earthquake using radar interferometry. Geophysical Research Letters 28 (6), 1079–1082.

Yu, T.-T., Rundle, J.B., Fernández, J., 1996a. Deformation produced by a rectangular dipping fault in a visco-elastic-gravitational layered Earth model—Part II: strike slip fault STRGRV and STRGRH FORTRAN programs. Computers & Geosciences 22 (7), 751–764 (corrigendum in Computers & Geosciences 28 (1), 89–91, 2002).

Yu, T.-T., Rundle, J.B., Fernández, J., 1996b. Surface deformation due to a strike-slip fault in an elastic gravitational layer overlying a viscoelastic gravitational half-space. Journal of Geophysical Research 101, 3199–3214 (correction: Journal of Geophysical Research 104 (B7), 15313–15315, 1999).